Journal of Korea Multimedia Society Vol. 15, No. 12, December 2012(pp. 1417-1429)

Segmentation of Neuronal Axons in Brainbow Images

Tae-Yun Kim†, Mi-Sun Kang††, Myoung-Hee Kim†††, Heung-Kook Choi††††

ABSTRACT

In neuroscientific research, image segmentation is one of the most important processes. The morphology of axons plays an important role for researchers seeking to understand axonal functions and connectivity. In this study, we evaluated the level set segmentation method for neuronal axons in a Brainbow confocal microscopy image. We first obtained a reconstructed image on an x - z plane. Then, for preprocessing, we also applied two methods: anisotropic diffusion filtering and bilateral filtering. Finally, we performed image segmentation using the level set method with three different approaches. The accuracy of segmentation for each case was evaluated in diverse ways. In our experiment, the combination of bilateral filtering with the level set method provided the best result. Consequently, we confirmed reasonable results with our approach; we believe that our method has great potential if successfully combined with other research findings.

Key words: Brainbow, Confocal microscopy image, Image segmentation, Level set method, Anisotropic diffusion, Bilateral filtering

1. INTRODUCTION

The discovery of the jellyfish green fluorescent protein (GFP) as a vital stain has enabled researchers to stain individual axons. Because the GFP chromophore is derived entirely from the polypeptide chain, GFP can be used to label living cells with minimal perturbation. Researchers have been using yellow fluorescent protein (YFP), a spectral variant of GFP, to label axons in vivo. In earlier works, combining two fluorescent protein (XFPs) in one animal and stably expressing them in a mosaic manner has been achieved through various strategies. However, these approaches are cumbersome and generate only a limited palette of colors.

In 2007, Lichtman and Sanes developed the “Brainbow” technique [1]. Brainbow is a term coined to describe a process by which individual neurons of a brain are mapped with fluorescent proteins that cause the neurons to glow with specific colors under a light source. By controlling and varying the amount of red, green, and blue derivatives of XFPs expressed in individual neurons, it is possible to map each neuron with a distinctive color. Earlier techniques allowed for mapping only a few neurons; the new method allows more than 100 different neurons to be simultaneously mapped in this manner. The resulting images can be quite striking and have, in fact, won awards in science

※ Corresponding Author : Heung-Kook Choi, Address : Injero 197, Department of Computer Engineering, Inje University, Gim-Hae, Gyeong-Nam 621-749, Rep. of Korea, TEL : +82-55-320-3437, FAX : +82-55-322-3107, E-mail : cschk@inje.ac.kr
Receipt date : Jul. 18, 2012, Revision date : Sep. 7, 2012
Approval date : Sep. 17, 2012
† Biomedical Engineering Branch, National Cancer Center, (E-mail: liminus@daum.net)
†† Department of Computer Science and Engineering, Ewha Womans University
(E-mail: Mesun@ewhain.net)
††† Department of Computer Science and Engineering, Ewha Womans University
(E-mail: mhkim@ewha.ac.kr)
†††† Department of Computer Engineering, UHRC, Inje University
※ This work was supported by the National Research Foundation of Korea (NRF) grant funded by the Korea government (MEST) (No. 20100000771) and Korea Institute for Advancement of Technology (KIAT) through the Human Resource Training Project for Strategic Technology.

photography competitions.

Image segmentation is an essential step in understanding image content because the quality of the interpretation of image visual objects depends on the results of image segmentation. This process divides an image into different regions such that each region is homogeneous and the borders between adjacent regions are distinct. Studies of image segmentation have been performed previously, and notable examples are the Snake model proposed by Kass, Witkin, and Terzpoulos [2] and the region-growing method proposed by Beveridge et al. [3]. Furthermore, many studies have been performed to improve these traditional approaches [4-6].

In neuroscientific research, image segmentation is one of the most important processes. The morphology of axons plays an important role in understanding axonal functions and connectivity. Tracking and extracting the axons requires correctly segmenting axons from the background and separating each axon from its neighborhood. However, traditional methods of manual segmentation and tracking of axons are tedious, requiring hours of careful labeling and correction. Many methods of segmenting and tracking various tubular objects such as axons and vessels or other neuronal structures accurately and rapidly have been reported recently [7-12]. Cai et al. studied the repulsive-force-based active-contour method for tracking axons [13], and Srinivasan et al. proposed a probabilistic region-merging-based method for axon centerline detection [14]. Cohen et al. presented a method for automatic three-dimensional (3D) tracing from confocal image stacks of selectively stained neurons based on segmentation, skeletonization, and graph extraction [15]. For curvilinear structure detection, Wang et al. studied a dynamic local tracing method by considering local neuronal topology [16]. Vasilevskiy and Siddiqi and Nain et al. developed a geometric-flow framework to perform 2D and 3D vessel segmentation using prior knowledge of the vessel shape [17-18]. Vazquez-Reina et al. proposed the multiphase, level set, active ribbon model, which segmented multiple objects simultaneously by combining several level set functions [19]. Jeong et al. also proposed an improved algorithm that solves the sensitivity problem during contour initialization by adding an additional constraint [20]. Recently, Jurrus et al. purposed a novel axon-tracking method based on the Kalman filter [21].

The major purpose of the present study was to investigate axon segmentation methods as a prephase of 3D axon reconstruction. To do this, we evaluated accuracy and speed in segmentation, combining the level set segmentation method with bilateral and anisotropic filtering.

Section 2 describes the research material along with the details about obtaining the images used in the experiment and methods. Section 3 presents the study results from the application of the method to the actual Brainbow confocal microscopy image data and an evaluation of the results, followed by conclusions in the final section.

2. METHODS

2.1 Materials

Original Brainbow confocal microscopy images were provided by Department of Radiology, Methodist Hospital Research Institute, Weill Medical College of Cornell University. Brainbow constructs were assembled using standard cloning methods with the nine XFPs. For transgenic mouse generation, Brainbow constructs were cloned in a *Thy1.2* cassette. Mice were anaesthetized with sodium pentobarbital before intracardiac perfusion with PBS and 4% PFA. Then 100-μm sagittal brain sections were obtained using a vibrating microtome (Leica VT1000). Sections and fixed tissues were mounted in Vectashield and stored at -20°C before imaging.

Fixed-brain and muscle samples were imaged

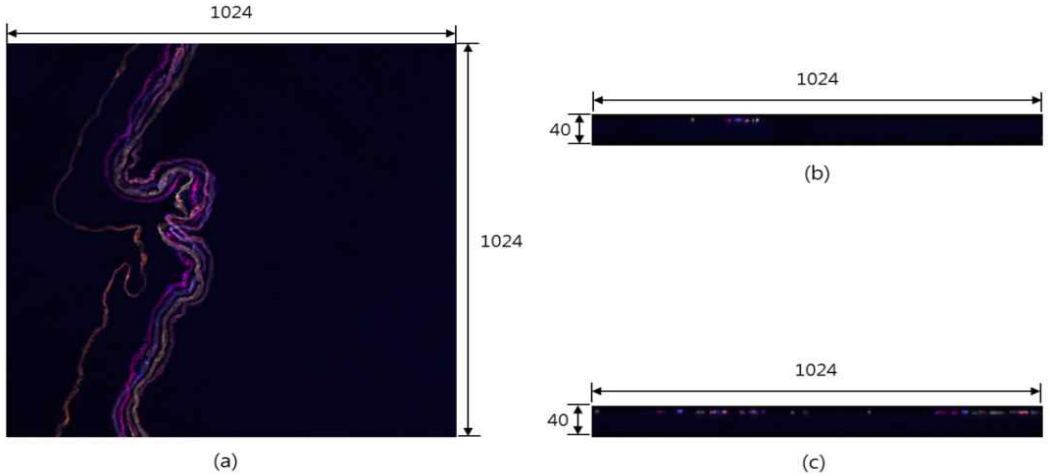

Fig. 1. Image stacks: (a) x - y, (b) x - z, and (c) y - z plane.

with ×20 (0.8 NA), ×40 (1.3 NA), or ×60 (1.45 NA) oil objectives. Confocal images were acquired with an Olympus FV1000 microscope equipped with a 440-, 515-, 568-, and 633-nm primary beam splitter using a 440-nm photodiode laser for cyan fluorescence protein (CFP; PMT1, 510 nm, dichroic mirror, 465 - 495-nm barrier filter), a 515-nm argon line for YFP (PMT2, 560-nm dichroic mirror, 530 - 565 nm barrier filter), and a 561-nm photodiode laser or 568-nm krypton laser for red fluorescence protein (RFP; PMT3, 568 - 615-nm barrier filter). Confocal image stacks for all three channels were acquired sequentially and were maximally projected.

The original x - y plane Brainbow image sets were composed of about 40 slices, each with a size of 1024×1024 pixels and a resolution of 24 bits/pixel. These images were reconstructed to gray images with 8 bits per pixel and then used for image segmentation using the following formula as

$$gray\ level = \sqrt{red^2 + green^2 + blue^2}/\sqrt{3} \quad (1)$$

Although the spectral information is essential in Brainbow image, we just focused on the selection of proper segmentation method, so we performed gray scale based image segmentation.

Original x-y plane volume data was reconstructed as new stacks on x-z and y-z planes additionally. Fig. 1 presents examples of cross-sectional images of stacks on $x-y$, $x-z$, and $y-z$ planes, respectively. Then, we selected the x-z plane stack after investigation, with the easy accessibility of individual axon object and mainly performed our analysis on this plane.

2.2 Overall pipeline procedures

The overall procedure for this study is summarized in Fig. 2. First, we performed a preprocessing step using anisotropic diffusion and bilateral filtering. These two filters can preserve edges while unwanted image artifacts such as noise are smoothed or removed effectively.

When using a filtering method for medical image data, image degradation caused by blurring or artifacts resulting from a filtering scheme is not acceptable. However, preprocessing sometimes modifies texture or image information in unintended ways. Therefore, the following three requirements should ideally be fulfilled:

- Minimize information loss by preserving ob-

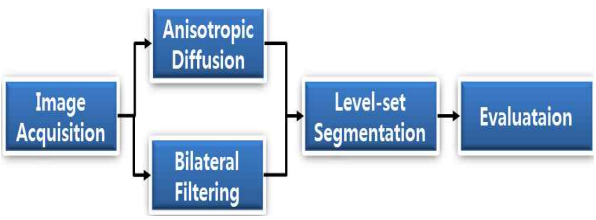

Fig. 2. Overall pipeline procedures.

ject boundaries and the detailed structure.
- Efficiently remove noise in regions of homogeneous physical properties.
- Enhance morphological definition by sharpening discontinuities.

A necessary denoising process should be applied to the image to remove noise contained in the image before any further processing. Regarding noise reduction, well known filtering techniques such as mean or median filtering can be used easily but these techniques lack image feature preservation. And general linear low-pass filters, such as the Gaussian filter, also smooth both noise and high-frequency information from edges. Therefore, more advance methods are needed to preserve and enhance edge information during the denoising process.

Moreover, in the case of level-set method, it is very important to consider this issue. For example, a local minimum of energy such as spurious edges caused by noise may stop the evolution of the active contour unexpectedly. In addition, when we enhance image edges effectively, total computational cost of the level set method also can be reduced.

We confirmed the effectiveness of two denoising filters from the result of our preliminary study. Fig. 3 below shows a result of denoising test by applying three different types of filters (anisotropic diffusion, bilateral and Gaussian smoothing). Although the Gaussian filter removed noises effectively, it couldn't preserve edges at the same time. On the contrary, other two filters showed relatively reasonable results. According to the result of our test, we selected these two approaches for preprocessing.

Then we segmented images using active contour based on the level set method. Finally, we performed comparative evaluations of the segmentation accuracy for each case.

2.3 Anisotropic Diffusion Filtering

The first preprocessing method applied in this study was anisotropic diffusion filtering [22-23]. This is a powerful scheme for multi-scale description of images, image segmentation, edge detection, and image enhancement. The basic idea of anisotropic diffusion is to evolve from an original image $u_0(x,y)$ $u_0(x,y)$, defined in a convex domain $\Omega \subset R \times R$, to a family of increasingly smooth images u(x,y,t) derived from the solution of the following partial differential equation:

$$\frac{\partial u}{\partial t} = \mathrm{div}[D(|\nabla u|)\nabla u] \quad (2)$$

with initial condition u(x,y,0)=u(x,y). The diffusion coefficient D(・) is a nonnegative function of the magnitude of local image gradient $|\nabla u| = \sqrt{u_x^2 + u_y^2}$. The desirable diffusion coefficient in Equation 2

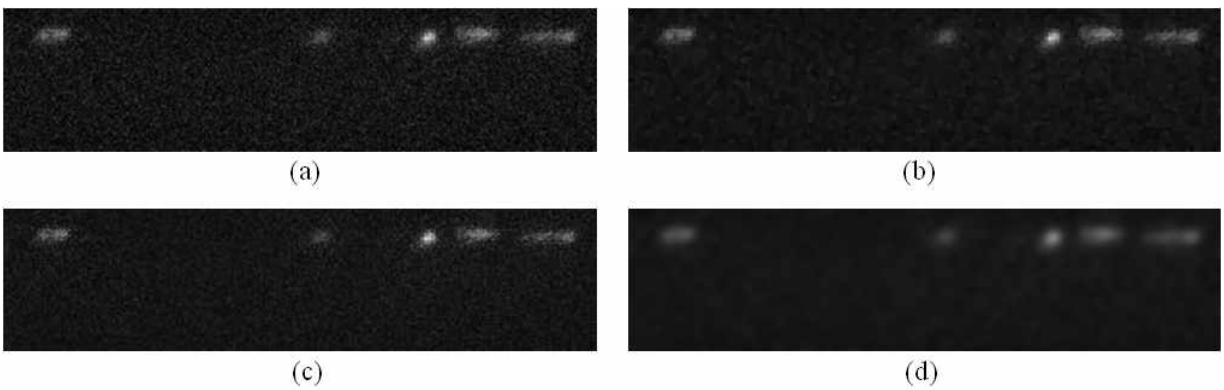

Fig. 3. An example of preprocessing results on the Brainbow image: (a) original Image (b) bilateral filtering; (c) anisotropic diffusion filtering; and (d) Gaussian filtering

diffuses more in smooth areas and less around large intensity transitions, so that small variation in image intensity such as noise and unwanted texture are smoothed and edges are preserved. Two different functions have been proposed:

$$D(s) = \exp\left[-\left(\frac{s}{k}\right)^2\right] \quad (3)$$

$$D(s) = \frac{1}{1+\left(\frac{s}{k}\right)^2} \quad (4)$$

The parameter k is chosen according to noise level and edge strength. In this study, we empirically selected the formula (Eq. 3) as a conduction coefficient function, and set iteration number to 30, kappa (k) values to 30, and ∇u to 0.14, respectively, and applied the filter to each image slice-by-slice.

2.4 Bilateral Filtering

As another preprocessing method, we used bilateral filtering. Originally, bilateral filtering was proposed as a noniterative alternative to anisotropic diffusion [24-26]. Unlike anisotropic diffusion, bilateral filtering does not involve the solution of partial differential equations, and it can be implemented in a single iteration. It combines gray levels or colors based on both their geometric closeness and their photometric similarity, and prefers near values to distant values in both domain and range. Bilateral filtering involves a weighted convolution in which the weight for each pixel depends not only on its distance from the center pixel but also its relative intensity. A simple case of bilateral filtering is shift-invariant Gaussian filtering, in which filter components are Gaussian functions of Euclidean distance. Two filter components, the closeness function c(,x) and the similarity function s(,x), are defined as follows:

$$c(\xi, x) = e^{-\frac{1}{2}\left(\frac{d(\xi,x)}{\sigma_d}\right)^2} \quad (5)$$

where $d(\xi, x) = d(\xi - x) = \|\xi - x\|$ is the Euclidean distance between ξ and x.

$$s(\xi, x) = e^{-\frac{1}{2}\left(\frac{\delta(f(\xi), f(x))}{\sigma_r}\right)^2} \quad (6)$$

where $\delta(i, j) = \delta(i - j) = \|i - j\|$ is a measurement between the two intensities i and j. The geometric spread σ_d in the domain is chosen based on the desired amount of low-pass filtering. A large σ_d blurs more; in other words, it combines values from more distant image locations. Similarly, the photometric spread σ_r in the image range is set to achieve the desired amount of combination of pixels. Pixels with values much closer to each other than σ_r are combined. In our case, it showed best results when we selected two parameter values as σ_d=3 and σ_r=10 empirically.

2.5 Level-set based Segmentation

Traditional active contour models can be classified as either parametric models or geometric models according to their representation and implementation. Geometric models, introduced by Caselles et al. are based on curve-evolution theory and the level set method [27]. The classical models have some limitations. They are nonintrinsic because the energy depends on the parameterization of the curve, and they are not directly related to the object geometry. To avoid these limitations inherent to the active-contour model, level sets can be used, which provide an implicit representation of the curve [28-30]. Level-set based segmentation provides a well-known to encode segment boundaries at a homogeneous resolution, with simple up- and down-sampling scheme. In addition, in the case of multiple objects, the detection and formulation of constraints to prevent overlaps between adjacent segment boundaries can be achieved much simpler by a level set function where signed distance functions are employed. In this reason, we adapted the level-set based active contour model method for our purpose.

The two most common categories of Level set methods are the "active contour with edge" approach and the "active contour without edge" approach.

The main advantages of using level sets are that

arbitrarily complex shapes can be segmented and topological changes such as merging and splitting are handled implicitly. The basic idea is summarized as follows:

1. Instead of manipulating the contour directly, the contour is embedded as the zero level set of function, called the level set function $\phi(x,t)$.
2. The surface intersects the image at the location of the curve. As the curve is at height 0, it is called the zero level set of the surface.
3. The higher dimensional level set function is then evolved under the control of a partial differential equation (PDE) instead of the original curve.
4. The zero level set remains identified with the curve during evolution of the surface. At any time, the evolving contour can be obtained by extracting the zero level set $\phi(x,t)=0$ from the output.

Li et al. proposed a new variational formulation for geometric active contours that forces the level set functions to be close to a signed distance function, and therefore completely eliminates the cost of re-initialization [31]. In this study, we applied their approach to improve the segmentation performance. For applying the level-set based active contour segmentation in practical, several initial parameters were set empirically.

1. Scale parameter in Gaussian kernel for smoothing (σ): 1.5
2. Smoothing parameter in the Dirac function (ε): 1.5
3. Time step of curve evolution (t): 5
4. The coefficient of the internal energy term (μ): 0.15
5. The coefficient of the weighted length term (λ): 5
6. The coefficient of the weighted area term (ϕ): 3

We also selected total six numbers of iterations(100, 200, 250, 300, 350, and 400) for comparing computational costs and tested for each case.

2.6 Measurement of Image Similarity

Generally, the best-known methods for similarity measurement include Sum of Squared Distance (SSD) based on the difference of pixel intensities, Sum of Absolute Distance (SAD), Normalized Correlation Coefficient (NCC) based on the correlation, and Mixed Pixel Count (MPC) based on the number of similar pixels [32-35].

In this study, we measured similarity by using Mean Square Error (MSE), Peak Signal-to-Noise Ratio (PSNR), and NCC. MSE and PSNR are the most common measures of image similarity, despite of the fact that they are not adequate as perceptually meaningful measures. A high MSE value means that there is a high degree of difference from the original image, and this indicates low similarity because it is measured as a low PSNR value. A low MSE value signifies little difference from the original image, and it is measured as high PSNR, indicating high similarity. NCC is a measurement parameter that can complement well-known cross-correlation methods. Furthermore, NCC overcomes limitations by normalizing the image and template vectors to unit length, yielding a cosine-like correlation coefficient.

$$\mathrm{MSE} = \frac{1}{MN}\sum_{i=1}^{M}\sum_{k=1}^{N}(x_{j,k}, y_{j,k})^2 \tag{7}$$

$$\mathrm{PSNR} = 10\log\frac{(2^n-1)^2}{\mathrm{MSE}} \tag{8}$$

$$\mathrm{NCC} = \sum_{i=1}^{M}\sum_{k=1}^{N} x_{j,k} \cdot y_{j,k} \,/\, \sum_{i=1}^{M}\sum_{k=1}^{N} x_{j,k}^2 \tag{9}$$

where M and N indicate the size of the image in rows and columns, respectively. i and k represent the pixel coordinates, and $x_{j,k}$, $y_{j,k}$ represent the pixel values of the original and segmented images, respectively.

3. RESULTS

The experimental result using the Brainbow im-

ages describes the detailed evaluations. Fig. 4 presents the different results of bilateral filtering with variations in range and domain parameters (σ_r,σ_d). Rows correspond to different amounts of domain filtering, while columns correspond to different amounts of range filtering. When the σ_r is large with respect to the overall range of values in the image, the range component of the filter has little effect for small σ_d. For smaller values of the range parameter σ_r, range filtering dominates perceptually because it preserves edges.

We compared segmentation times based on the number of iterations of the level set method. We performed level set segmentations using the original image without preprocessing, the image with anisotropic diffusion, and the image with bilateral filtering. Fig. 5 and 6 present examples of each of these approaches. Red lines for each image show the result of the segmentation.

All images in Fig. 5 and 6 are partial 316×76 images extracted from x-z reconstructed images (1024×40) and magnified. Axon objects of original images are spread widely on the images regions. In this paper, we just focus on the accuracy of segmentation. We set a fixed ROI size and extracted a part of region for our study. Additionally, when we had used original image, it was also difficult to apply the level-set base method directly because height of the image is very small. In this reason, we magnified the extracted ROI patch images by 316×76. The visual investigation shows five objects (axons). Each row image represents the processes of level-set based segmentation according to each of the three approaches, by the number of iterations: 100, 200, 250, 300, 350, and 400, respectively. In the case of the first column in figure 5, which directly applied the level set method to original image, did not yield a reasonable result despite more than 400 iterations, except for the first object on the left. According to the intensities of background, contour failures occurred even though no object existed, as shown in second contour of the first column.

In contrast, the second (b) and third (c) columns, which used bilateral filtering and anisotropic diffusion as preprocessing, showed good results for the five objects, with effective edge preservation and smoothing despite smaller numbers of iterations. In the case of the second row (250 iterations), although it appears that anisotropic diffusion was faster than bilateral filtering, the anisotropic diffusion algorithm itself had additional iteration costs (in our case, 30) in application. For this reason, the case of bilateral filtering, which required no iteration itself, performed segmentation faster. Another test case in Fig. 6 also showed a similar tendency with the result of Fig. 5.

To compare image-segmentation accuracy, we performed segmentations on the same objects and accumulated each result contour with different colors. As a basis for comparison to evaluate the accuracy of segmentation, we used images man-

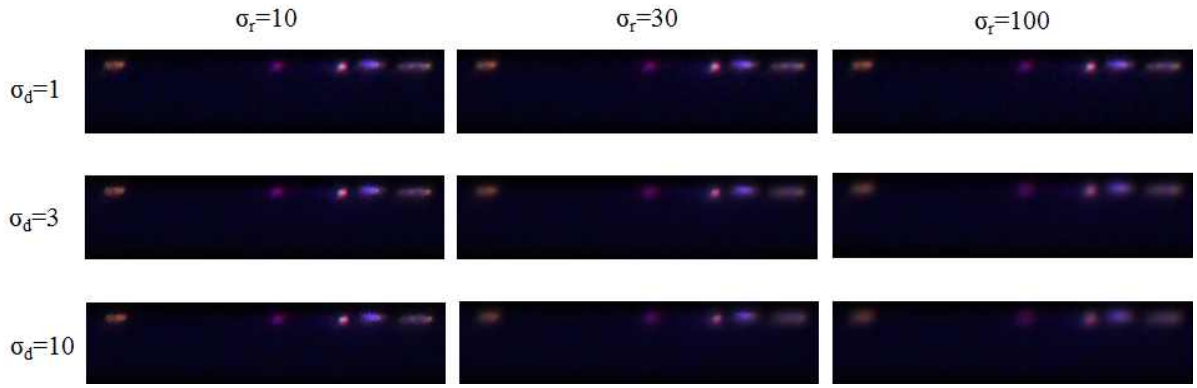

Fig. 4. Result of bilateral filtering with variations of range and domain parameters (σ_r, σ_d)

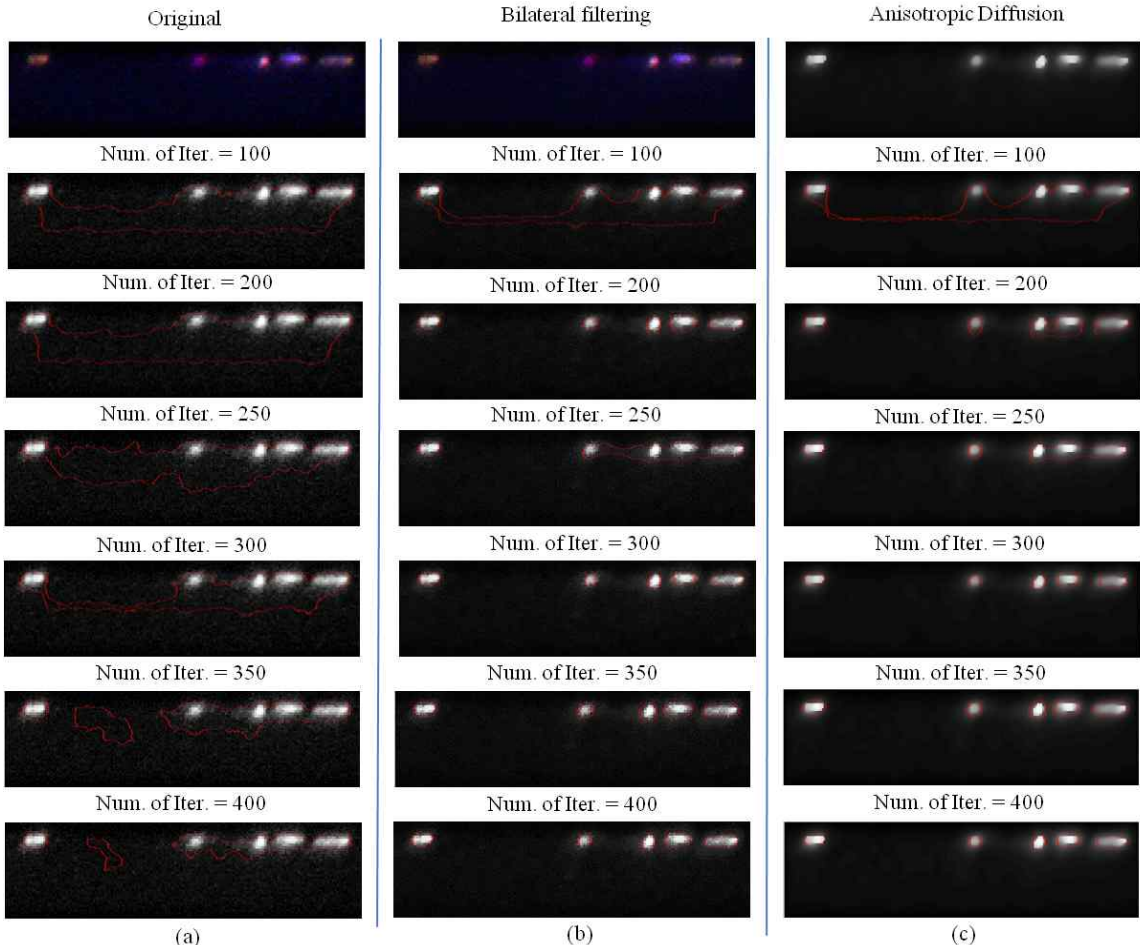

Fig. 5. A comparison of iteration costs for level set based three approaches #1: (a) Level-set method using original image (b) Level-set method after bilateral filtering, and (c) Level-set method after anisotropic diffusion filtering.

ually segmented by diagnosticians. By the nature of original image data, a gold standard to evaluate the accuracy didn't exist. In this reason, we had to use manual segmentation results as a standard. ROI drawing was supported by the open source software ImageJ (National Institutes of Health (NIH), USA).

Fig. 7 below shows an example of one such image overlaid with each segmented contour from the original image.

As we can see, the blue contour (bilateral filtering) is most similar to the result of manual segmentation, and the green contour (anisotropic diffusion filtering) showed a slight tendency toward under-segmentation.

Finally, the evaluation more objectively measured the similarity between the original and segmented images using the aforementioned three parameters. Table 1 summarizes average values of

Table 1. A summary of similarity measurements for the three approaches

Specification of two input image	Measurement	
(Manual) - (Original + Level-Set)	MSE	90.6546
	PSNR	28.5569
	NCC	0.2500
(Manual) - (Anisotropic Diffusion + Level-Set)	MSE	32.7192
	PSNR	32.9828
	NCC	0.4144
(Manual) - (Bilateral Filtering + Level-Set)	MSE	9.5334
	PSNR	38.3383
	NCC	0.7413

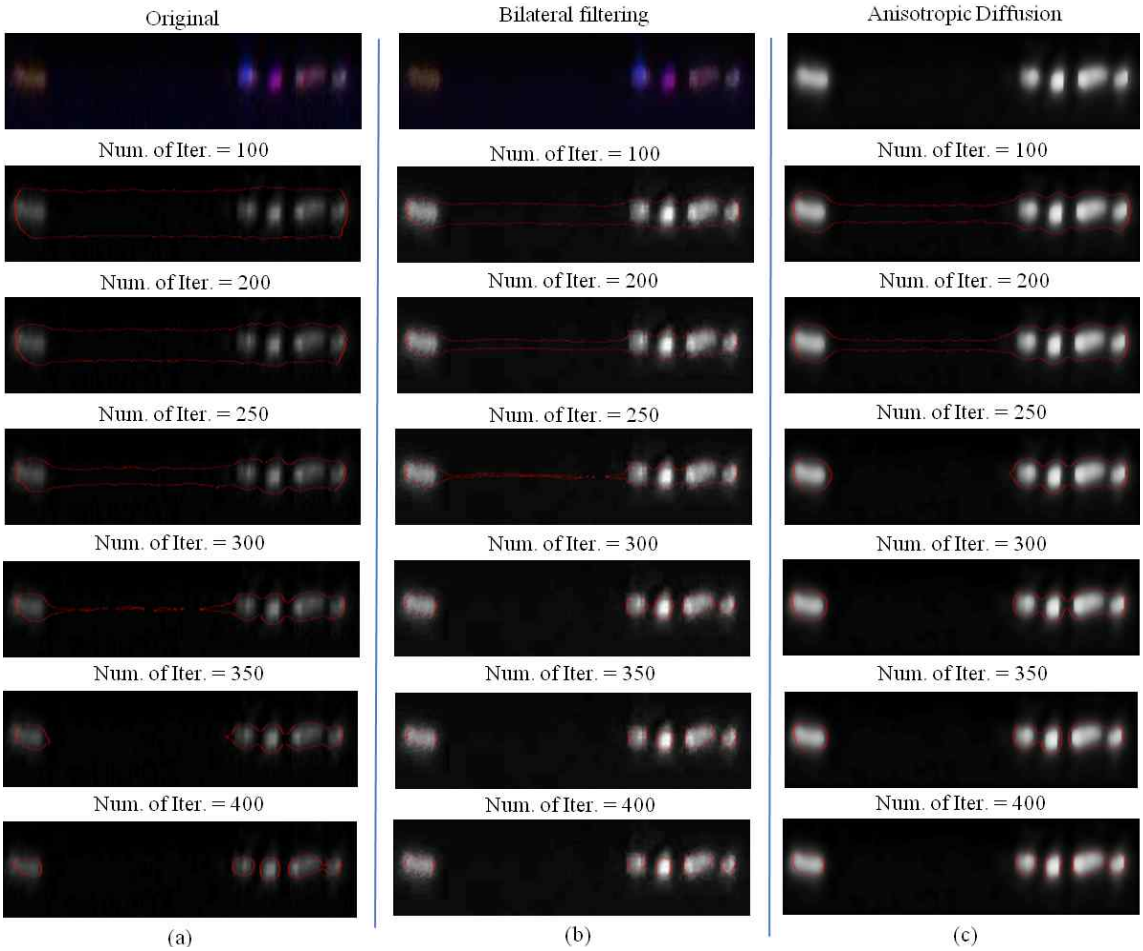

Fig. 6. A comparison of iteration costs for level set based three approaches #2: (a) Level-set method using original image (b) Level-set method after bilateral filtering, and (c) Level-set method after anisotropic diffusion filtering.

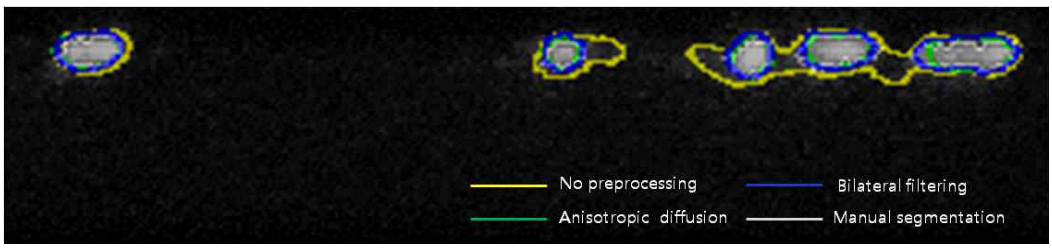

Fig. 7. An overlay image of segmentation results (corresponding to the Fig. 5).

three different similarity parameters for 10 serial images using original images and segmented images from the three approaches. As we expected, the image segmented after bilateral filtering scored the highest PSNR values (38.3383) and lowest MSE values (9.5334), so we confirmed that the similarity of this technique to manual segmentation is relatively high. It also scored the highest NCC values (0.7413) among the three cases.

4. CONCLUSION

The level set method can detect and segment multiple objects simultaneously. In this respect, we think that our approach is suitable for neuroscientific image segmentation for images such as

Brainbow images. However, contour initialization failure occurred from several test data when we performed the experiment. These errors must be analyzed in detail. In most cases, we solved this problem by adjusting the control parameters of the preprocessing methods. However, some of test images with high background variation or low contrast still need to be improved. In addition, to segment axons with occurrence windings of objects frequently on planes at different angles, and to visualize them in 3D space, the center line extraction approaches reported in recent research should be considered. The method proposed by Srinivasan et al. is a good example [14]. In this method, they extracted the center line of axons using the x - y plane MIP images combined with cross-sectional images, and they successfully reconstructed 3D volume data. To effectively visualize many objects with more than 100 different colors, the application of 3D labeling techniques is important. Unlike color image segmentation, in cases of gray-level image segmentation, such as our approach, we should necessarily consider this process. We applied 3D labeling in our previous study on visualization based on surface rendering and analysis of cancer-cell nuclei and obtained successful results [36-37].

The main purpose of this paper has been to explore the possibility for accurately segmenting axons in Brainbow confocal microscopy images and evaluating the results through diverse measurements. The results of our study show that the combination of bilateral filtering with the level set method produces the best result. These results were evaluated using various measurements of the level-set based three different approaches. Certainly, the present study was limited in scope. Further studies with different, large-scale assessments are needed. However, the results of this study point to several promising directions for future research. We believe that our method, in combination with other research findings, has great potential.

REFERENCES

[1] J. Livert, T.A. Weissman, H.O. Kang, R.W. Draft, J. Lu, R.A. Bennis, J.R. Sanes, and J.W. Lichtman, "Transgenic Strategies for Combinatorial Expression of Fluorsescent Proteins in the Nervous System," *Nature,* Vol. 450, No. 7166, pp. 56-63, 2007.

[2] M. Kass, A. Witkin, and D. Terzopoulos, "Snakes: Active Contour Models, *International Journal of Computer Vision,* Kluwer Academic Publishers, Boston, 1988.

[3] J.R. Beveridge, J. Griffith, R.R. Kohler, A.R. Hanson, and E.M. Riseman, Segmenting Images Using Localizing Histograms and Region Merging, *International Journal of Computer Vision,* Kluwer Academic Publishers, Boston,, 1989.

[4] R. Adams and L. Bischof, "Seeded Region Growing," *IEEE Trans Pattern Analysis Machine Intell* Vo. 16, No. 6, pp. 641-647, 1994.

[5] R. Grzeszczuk and D. Levin, "Brownian Strings: Segmenting Images with Stochastically Deformable Contours," *IEEE Trans Pattern Anal Machine Intell,* Vol. 19, No. 10, pp. 1100-1114, 1997.

[6] S. Lankton and A. Tannenbaum, "Localizing Region-based Active Contours," *IEEE Trans Image Proc.*, Vol. 17, No. 11, pp. 2029-2039, 2008.

[7] F. Benmansour and L.D. Cohen, "Tubular Structure Segmentation Based on Minimal Path Method and Anisotropic Enhancement,: *Int J. Comput Vision*, Vol. 92, No. 2, pp. 192-210, 2011.

[8] L.M. Lorigo, O.D. Faugeras, W.E.L. Grimson, R. Keriven, R. Kikinis, A. Nabavi, and C.F. Westin, "Curves: Curve Evolution for Vessel Segmentation," *Med Image Anal,* Vol. 5, No.

3, pp. 195-206, 2001.

[9] D. Marín, A. Aquino, M.E. Gegundez-Arias, and J.M. Bravo, "A New Supervised Method for Blood Vessel Segmentation in Retinal Images by Using Gray-Level and Moment Invariants- Based Features," *IEEE Trans Med Imaging*, Vol. 30, No. 1, pp. 146-158, 2011.

[10] C.C. Reyes-Aldasoro, L.J. Williams, S. Akerman, C. Kanthou, and G.M. Tozer, "An Automatic Algorithm for the Segmentation and Morphological Analysis of Microvessels in Immunostained Histological Tumour Sections," *J. Microscopy*, Vol. 242, No. 3, pp. 262-278, 2011.

[11] J.V.B. Soares, J.J.G. Leandro, R.M. Cesar, H.F. Jelinek, and M.J. Cree, "Retinal Vessel Segmentation Using the 2-D Gabor Wavelet and Supervised Classification," *IEEE Trans Med Imaging,* Vol. 25, No. 9, pp. 1214-1222, 2006.

[12] Y. Zhang, K. Chen, M. Baron, M.A. Teylan, Y. Kim, Z. Song, P. Greengard, and S.T.C. Wong, "A Neurocomputational Method for Fully Automated 3D Dendritic Spine Detection and Segmentation of Medium-Sized Spiny Neurons," *NeuroImage,* Vol. 50, No. 4, pp. 1472-1484, 2010.

[13] H. Cai, X. Xu, J. Lu, J.W. Lichtman, S.P. Yung, and S.T.C. Wong, "Repulsive Force Based Snake Model to Segment and Track Neuronal Axons in 3D Microscopy Image Stacks," *NeuroImage* Vol. 32, No. 4, pp. 1608-1620, 2006.

[14] R. Srinivasan, X. Zhou, E. Miller, J. Lu, J. Lichtman, and S.T.C. Wong, "Automated Axon Tracking of 3D Confocal Laser Scanning Microscopy Images Using Guided Probabilistic Region Merging," *Neuroinformatics,* Vol. 5, No. 3, pp. 189-203, 2007.

[15] A.R. Cohen, B. Roysam, and J.N. Turner, "Automated Tracing and Volume Measurements of Neurons from 3-D Confocal Fluorescence Microscopy Data," *J. Microscopy,* Vol. 173, No. 2, pp. 103-114, 1994.

[16] J. Wang, X. Zhou, J. Lu, J. Lichtman, S.F. Chang, and S.T.C. Wong, "Dynamic Local Tracing for 3D Aaon Curvilinear Structure Detection from Microscopic Image Stacks," *Proc. 4th IEEE Int Symposium Biomed Imaging: From Nano to Macro,* pp. 81-84, 2007.

[17] A. Vasilevskiy and K. Siddiqi, "Flux Maximizing Geometric Flows," *IEEE Trans Pattern Anal Machine Intell,* Vol. 24, No. 12, pp. 1565-1578, 2002.

[18] D. Nain, A.J. Yezzi, and G. Turk G, "Vessel Segmentation Using a Shape Driven Flow," *Proc. Med Image Comput Computer Assisted Intervention* pp. 51-59, 2004.

[19] A. Vazquez-Reina, E. Miller, and H. Pfister, "Multiphase Geometric Coupling for the Segmentation of Neural Processes," *Proc. IEEE Comput Soc Conf Comput Vision Pattern Recog (CVPR2009),* pp. 2020-2027, 2009.

[20] W.K. Jeong, J. Beyer, M. Hadwiger, A. Vazquez, H. Pfister, and R.T. Whitaker RT, "Scalable and Interactive Segmentation and Visualization of Neural Processes in EM Datasets," *IEEE Trans Visual Comput Graph,* Vol. 15, No. 1, pp. 1505-1514, 2009.

[21] E. Jurrus, M. Hardy, T. Tasdizen, P.T. Fletcher, P. Kpshevoy, C.B. Chien, W. Denk, and R. Whitaker, "Axon Tracking in Serial Block- face Scanning Electron Microscopy," *Med Image Anal,* Vol. 13, No. 1, pp. 180-188, 2009.

[22] F. Liu and J. Liu, "Anisotropic Diffusion for Image Denoising based on Diffusion Tensors," *J Vis Comm. and Image Rep.*, Vol. 23, No. 3, pp. 516-521, 2012.

[23] P. Perona and J. Malik, "Scale-space and Edge Detection Using Anisotropic Diffusion," *IEEE*

Trans Pattern Anal Machine Intell, Vol. 12, No. 7, pp. 629-639, 1990.

[24] D. Barash , "Bilateral Filtering and Anisotropic Diffusion: Towards a Unified Viewpoint," *Lecture Notes Comput Sci* 2006, pp. 273-280, 2006.

[25] F. Hofheinz, J. Langner, B. Beuthien-Baumann, L. Oehme, J. Steinbach, J. Kotzerke, and J. van den Hoff, "Suitability of Bilateral Filtering for Edge-preserving Noise Reduction in PET," *EJNMMI Research*, Vol. 1, No. 1, pp. 1-9, 2011.

[26] C. Tomaci and R. Mabduchi, "Bilateral Filtering for Gray and Color Images," *Proc. 6th IEEE Int Conf Comput Vision,* pp. 839-846, 1998.

[27] V. Caselles, F. Catte, T. Coll, and F. Dibos, "A Geometric Model for Active Contours in Image Processing," *Numerische Math,* Vol. 66, No. 1, pp. 1-31, 1993.

[28] O. Gloger, K.D. Tonnies, V. Liebscher, B. Kugelmann, R. Laqua, and H. Volzke, "Prior Shape Level Set Segmentation on Multistep Generated Probability Maps of MR Datasets for Fully Automatic Kidney Parenchyma Volumetry," *IEEE Trans Med Imaging*, Vol. 31, No. 2, pp. 312-325, 2012.

[29] J. Sethian, "A Fast Marching Level Set Method for Monotonically Advancing Fronts," *PNAS,* Vol. 93, No. 4, pp. 1591-1595, 1996.

[30] L.A. Vese and T.F. Chan, "A Multiphase Level Set Framework for Image Segmentation Using the Mumford and Shah Model," *Int J Computer Vision,* Vol. 50, No. 3, pp. 271-293, 2002.

[31] C. Li, C. Xu, C.F. Gui, and M.D. Fox, "Level Set Evolution without Re-initialization: A New Variational Formulation," *Proc. IEEE Comput Soc Conf Comput Vision Pattern Recog (CVPR'05),* Vol. 1, pp. 430-436, 2005.

[32] S. Grgic, M. Grgic, and M. Mrak, "Reliability of Objective Picture Quality Measures," *J Elect Eng,* Vol. 55, No. 55, pp. 3-10, 2004.

[33] J.P. Lewis, "Fast Template Matching," *Proc. Canadian Image Process Pattern Recog Soc Vision Interface,* pp. 120-123, 1995.

[34] M. Miyahara, K. Kotani, and V.R. Algazi, "Objective Picture Quality Scale (PQS) for Image Coding," *IEEE Trans Commun,* Vol. 46, No. 9, pp. 1215-1226, 1998.

[35] Y.M. Choi and M.W. Choo, "Comparison of Feature Selection Processes for Image Retrieval Applications, "*Journal of Korea Multimedia Society,* Vol. 14, No. 12, pp. 1544-1548, 2011.

[36] H.J. Choi, I.H. Choi, T.Y. Kim, N.H. Cho, and H.K. Choi, "Three-dimensional Visualization and Quantitative Analysis of Cervical Cell Nuclei with Confocal Laser Scanning Microscopy," *Anal Quant Cytol Histol,* Vol. 27, No. 3, pp. 174-180, 2005.

[37] T.Y. Kim, H.J. Choi, H.G. Hwang, and H.K. Choi, "Three-dimensional Texture Analysis of Renal Cell Carcinoma Cell Nuclei for Computerized Automatic Grading," *J. Med Syst,* Vol. 34, No. 4, pp. 709-716, 2010.

Tae-Yun Kim

He received the Ph.D. degree in Computer Science at the Department of Computer Science of Inje University in 2011. He is currently a researcher at National Cancer Center(NCC). His interesting research fields are in medical image analysis, medical image processing, and computer graphics.

Mi-Sun Kang

Mi-sun Kang received her B.S. degree(2007), M.S degree(2012) in Computer Science and Engineering at Ewha Womans University, Seoul, Korea. She is doing a Ph.D. in Computer Science and Engineering at Ewha Womans University. Her current research interests include cellular-image visual computing and biomedical image processing.

Myoung-Hee Kim

Myoung-Hee Kim received her Ph.D. degree (1986) from Universitaet Goettingen, Germany. She has been a professor in the Department of Computer Science and Engineering at Ewha Womans University, Korea, since 1987. Her current research interests include medical image segmentation, registration, visualization, simulation, and virtual reality.

Heung-Kook Choi

He has gone the undergraduate studying and graduate studying in computer science and engineering at the Department of Electrical Engineering of Linköping University, Sweden (1984-1990) and Ph.D. studying in computerized image analysis at the Center for Image Analysis of Uppsala University, Sweden (1990-1996). He was President of Industry and Academic Cooperation Foundation at Inje University and now he is Vice President of Korea Multimedia Society. His interesting research fields are in computer graphics, virtual reality, and medical image processing and analysis.